Earth and Space Science

RESEARCH ARTICLE
10.1029/2019EA000580

Key Points:
- This study presents a simulated ice cloud retrieval by a radar and multifrequency microwave radiometer space platform
- This combined active and passive remote sensing approach outperforms current state-of-the-art remote sensing of ice cloud properties
- It serves as a plausible candidate for future missions that target cloud and precipitation processes

Supporting Information:
- Supporting Information S1

Correspondence to:
J. H. Jiang,
jonathan.h.jiang@jpl.nasa.gov

Citation:
Jiang, J. H., Yue, Q., Su, H., Kangaslahti, P., Lebsock, M., Reising, S., et al. (2019). Simulation of remote sensing of clouds and humidity from space using a combined platform of radar and multifrequency microwave radiometers. *Earth and Space Science*, *6*, 1234–1243. https://doi.org/10.1029/2019EA000580

Received 4 FEB 2019
Accepted 15 JUN 2019
Accepted article online 25 JUN 2019
Published online 22 JUL 2019

Simulation of Remote Sensing of Clouds and Humidity From Space Using a Combined Platform of Radar and Multifrequency Microwave Radiometers

Jonathan H. Jiang[1], Qing Yue[1], Hui Su[1], Pekka Kangaslahti[1], Matthew Lebsock[1], Steven Reising[2], Mark Schoeberl[3], Longtao Wu[1], and Robert L. Herman[1]

[1]Jet Propulsion Laboratory, California Institute of Technology, Pasadena, CA, USA, [2]Microwave Systems Laboratory, Colorado State University, Fort Collins, CO, USA, [3]Science and Technology Corporation, Hampton, VA, USA

Abstract This study presents a simulated simultaneous retrieval of mass mean cloud ice particle effective diameter, ice water content, water vapor, and temperature profiles using a combination of a 94-GHz cloud radar and multifrequency (118, 183, 240, 310, 380, 664, and 850 GHz) millimeter- and submillimeter-wave radiometers from a space platform. The retrieval capabilities and uncertainties of the combined radar and microwave radiometers are quantified. We show that this combined active and passive remote sensing approach with SmallSat technologies addresses a gap in the current state-of-the-art remote sensing measurements of ice cloud properties, especially deriving vertical profiles of ice cloud particle sizes in the atmosphere together with the ambient thermodynamic conditions. Therefore, this new approach can serve as a plausible candidate for future missions that target cloud and precipitation processes to improve weather forecasts and climate predictions.

1. Introduction

Clouds and water vapor are strong modulators of Earth's hydrological cycle, weather, and climate (Hartmann & Short, 1980; Stephens, 2005; Bony et al., 2006). In 2017, an Earth Science Decadal Survey released by the U.S. National Academies outlined a 10-year planned scientific missions and goals summarized based on inputs from scientists in the United States and beyond. This 2017 Decadal Survey identified clouds, convection, and precipitation as one of the targeted observables that are essential to advancing our understanding of a broad range of Earth science themes. In particular, "For ice clouds, the challenge is even more daunting than for water clouds owing to serious gaps in knowledge of dynamics and microphysics." [https://www.nap.edu/catalog/24938/thriving-on-our-changing-planet-a-decadal-strategy-for-earth, *Thriving on our changing planet: A decadal strategy for Earth observation from space*, 2017; hereafter DS2017].

Microwave radiometric measurements of liquid and ice clouds have been available from both aircraft and satellite platforms for over three decades using millimeter-wave frequencies mostly below 190 GHz (e.g., Burns et al., 1997; Hong et al., 2005; Wilheit et al., 1982). At submillimeter frequencies above ~200 GHz, the signals are mostly due to scattering and absorption by ice cloud particles, with limited interference from liquid clouds and water vapor (Evans et al., 1998; Wu et al., 2006; Wu & Jiang, 2004). As the frequency increases (i.e., wavelength decreases), the sensitivity of microwaves to smaller ice particles increases. By observing radiances using multiple channels spanning the millimeter and submillimeter frequencies, it is feasible to measure a wide range of ice particle sizes and their mass densities. However, nadir-pointing microwave sensors have coarse vertical resolution due to their wide weighting functions (Jiang et al., 2017). The technique of using multifrequency millimeter- and submillimeter-wave instruments to retrieve the vertical structures of ice cloud water content and ice particle effective diameter, along with the associated atmospheric temperature and water vapor profiles, has been developed (e.g., Evans et al., 2012; Jiang et al., 2017).

Narrow beam, 94-GHz (W-band) radar has been used to provide fine-scale cloud information from both aircraft and spaceborne platforms (Li et al., 2004; Stephens et al., 2002). The high scattering efficiency and short-wavelength W-band radar enables high sensitivity for both liquid and ice cloud detection, and pulse timing provides excellent vertical resolution. W-band radars supplement microwave radiometers' ability to measure broad features of cloud mass and particle sizes by improving characterization of the vertical structure of clouds. Radar-radiometer combinations have been recommended by the

Table 1
Center Frequencies (GHz), Offsets (GHz), and Bandwidths (GHz) of the Microwave Radiometer Suite

Channel	Center frequency	± Offset frequency	Bandwidth
1	118.75	1.1	0.4
2	118.75	1.5	0.4
3	118.75	2.1	0.8
4	118.75	5.0	2.0
5	183.31	1.0	0.5
6	183.31	3.0	1.0
7	183.31	6.6	1.5
8	243.20	2.5	3.0
9	310.00	2.5	3.0
10	380.20	0.75	0.7
11	380.20	1.80	1.0
12	380.20	3.35	1.7
13	380.20	6.20	3.6
14	664.00	4.20	4.0
15	850.00	0.0	4.0

DS2017 to quantify ice cloud properties, ranging from thin cirrus to deep convective clouds with precipitating ice.

A recently developed Tropospheric Water and Cloud ICE (TWICE) passive CubeSat instrument (Kangaslahti et al., 2016; Ogut et al., 2018; Reising et al., 2016) shows the potential of miniaturized radiometers. TWICE uses three radiometer front ends to provide 14 channels with frequencies of 118, 183, 240, 310, 380, and 664 GHz. Jiang et al. (2017) demonstrates TWICE's ability to retrieve profiles of cloud ice particle mass mean effective diameter (D_e), ice water content (IWC), water vapor (H_2O), and temperature (T) from space. Jiang et al. (2017) show that TWICE has limited sensitivity to small ice particles (~50% uncertainty for ice clouds with column-mean $D_e < 100$ μm). TWICE vertical resolution is 3-5 km. To enhance TWICE's sensitivity to smaller ice particles and improve the retrieval of vertically resolved ice cloud properties, a new 850-GHz radiometer is being incorporated into the TWICE instrument. The addition of the 850-GHz frequency to TWICE increases its sensitivity to ice clouds that are optically thin. This upgraded TWICE instrument combines four radiometer front ends that can be further hosted together with a 94-GHz cloud radar in a small-satellite payload, which is named as ENTICE (Earth's NexT-generation ICE mission), to provide finely resolved ice cloud vertical structure together with the ambient thermodynamic conditions.

This paper presents a detailed simulation of the fundamental measurements from the ENTICE suite of combined active radar and multifrequency passive microwave and submillimeter radiometers to assess the sensitivity and accuracy of the retrievals. We select eight frequencies corresponding to a 94-GHz radar and a seven-frequency (94, 118, 183, 240, 310, 380, 664, and 850 GHz) passive microwave submillimeter radiometer suite. The 15 channels for the radiometer suite are shown in Table 1. The TWICE Forward Radiative Transfer Model and Retrieval System (Jiang et al., 2017) has been updated to facilitate the new combined radar-radiometer instruments, as described in section 2. The sensitivity analysis is presented in section 3. The simulated retrieval and uncertainty estimates are shown in detail in section 4. A summary and conclusion are provided in section 5.

2. Forward Radiative Transfer Model

To simulate the brightness temperature spectra and the radar reflectivity vertical profiles that would be observed by the ENTICE, forward radiative transfer calculations are performed using the vertical profiles of atmospheric temperature (T) and relative humidity (RH), as well as cloud IWC, liquid water content, and mass mean equivalent spherical effective diameter (D_e) generated by the Weather Research and Forecasting (WRF) model Version 3.8.1 (Skamarock et al., 2008). Since ozone (O_3) has absorption bands in the microwave frequencies, the tropical O_3 profile from a standard atmosphere is used in all calculations.

The forward model component is in the Forward Radiative Transfer Model and Retrieval System (FMRS) described in Jiang et al. (2017). FMRS was developed based on the Spherical Harmonics Discrete Ordinate Method for Plane-Parallel Data Assimilation (SHDOMPPDA) by Evans (2007); Evans et al. (2012). It has been updated to include the additional 850-GHz channel and the 94-GHz cloud radar. The radar reflectivity is calculated at 0.5-km vertical resolution. The radiometric brightness temperature spectra at the top of the atmosphere are calculated for the channels specified in Table 1 by performing unpolarized radiative transfer calculations with randomly oriented particles. Only a brief summary on the forward model is provided here since a more detailed description can be found in Jiang et al. (2017). A k-distribution method (Fu & Liou, 1992) is used to calculate the molecular absorption for given temperature, water vapor, and ozone profiles. The single scattering properties of hydrometeors, such as ice particles and spherical liquid particles for each channel, are incorporated into the model by using precalculated scattering lookup tables as a function of particle size distribution, shape, and ambient temperature. These tables are calculated using the discrete dipole approximation method (Evans & Stephens, 1995; Yurkin & Hoekstra, 2011) for ice particles and the Mie program for liquid particles. The Mie assumption is used for solid sphere particles. For nonspherical particles, including plate aggregates, sphere aggregates, and snow aggregates, the discrete dipole approximation is

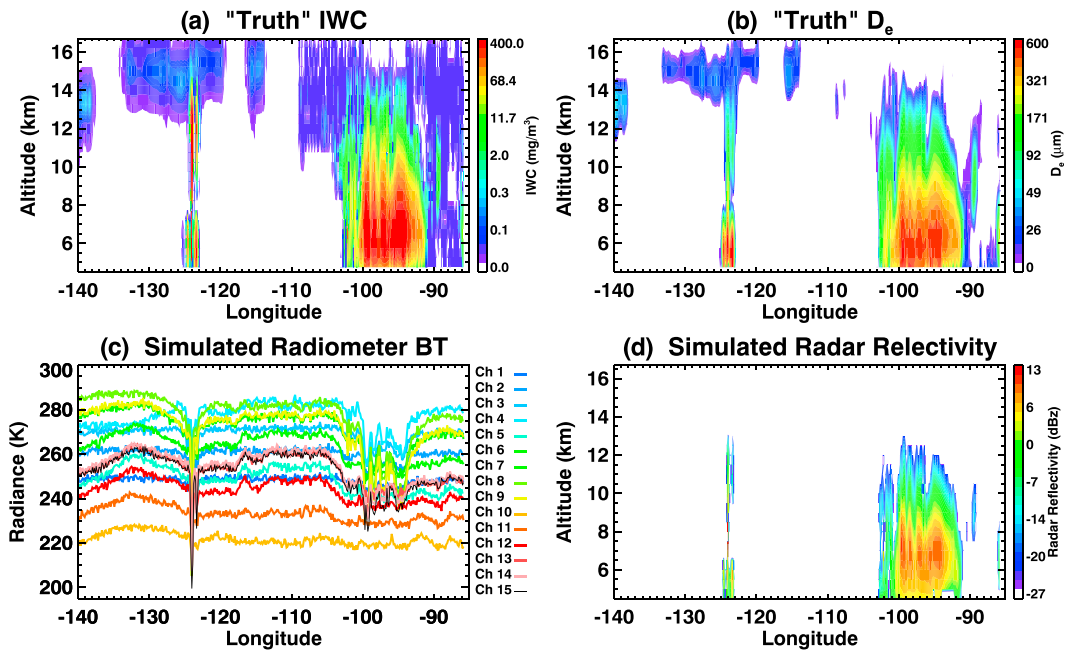

Figure 1. (a and b) The WRF simulated "Truth" ice water content (IWC) and D_e, respectively, along the cross section at 10°S between 140 and −85°W. (c and d) The forward model simulated radiance and reflectivity observations from the 15 passive radiometers channels and active 94-GHz radar, respectively, flying above with nadir viewing along the same cross section.

used. Since no ice particle shape information is readily available from the WRF, for the channel sensitivity study presented here, only the solid sphere shape is used for ice clouds in the forward calculation. A study by Wu et al. (2008) found that uncertainty of cloud induced radiances due to ice particle shape at microwave frequencies is generally less than 20%. The surface emissivity is assumed to be the value of Fresnel emissivity at ENTICE frequencies for a flat water surface at 26°C, plus 0.06 (Evans et al., 2012) to approximate ocean roughness.

To generate realistic atmospheric and cloud property profiles, a WRF model run is conducted with ~15-km horizontal resolution covering the entire globe with 50 levels in the vertical. The model simulation is initialized with the ERA-Interim (http://rda.ucar.edu/datasets/ds627.0/) at 1800 UTC on 31 May 2007. We use the simulation output at 0 UTC on 1 June 2007. The physical parameterizations include the Tiedtke scheme (Zhang et al., 2011) for convective processes, the Yonsei University scheme (Hong et al., 2006) for planetary boundary layer processes, the Rapid Radiative Transfer Model for General circulation model scheme (Iacono et al., 2008) for shortwave and longwave radiation, and the Thompson scheme (Thompson et al., 2008) for cloud microphysics. The liquid water content, IWC, rain, snow, and graupel, as well as their number concentration, are prognostically calculated in the model (Thompson et al., 2008). A sum of exponential and gamma distributions is used to represent the snow size distribution, while the size distribution of other hydrometeors is a generalized gamma distribution. Snow and ice cloud particles are differentiated by the effective size of the particle. Also produced by the WRF are the column integrated cloud ice water path (IWP), liquid water path, and column-integrated mass mean effective diameter (D_{me}).

A cross-section along the 10°S latitude between 140 and 85°W longitude is selected to illustrate the observations that would be obtained with ENTICE microwave radiometer channels and cloud radar. Both snow and ice cloud particles in the WRF simulation are included, such that the "truth" IWC is the summation of mass from both snow and ice cloud particles and the "truth" D_e is the average effective size weighted by the snow and ice cloud particle masses. As shown in Figure 1, this cross section includes a wide variety of ice clouds, such as thin cirrus, anvils, and deep convection with a range of ice particle sizes. Figures 1a and 1b show the WRF-simulated IWC and D_e profiles along this cross section, respectively. Figure 1c shows the forward model simulated top-of-atmosphere (TOA) radiances "observed" by the 15 microwave radiometer

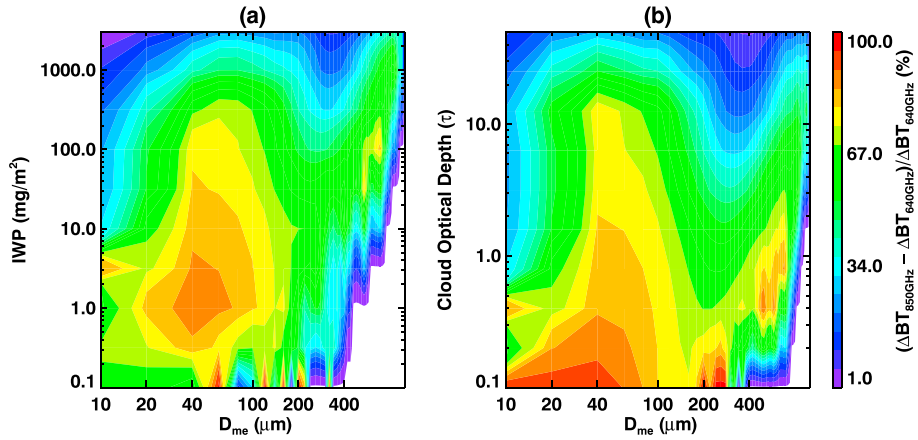

Figure 2. Simulated relative differences, (BT_{850GHz}-BT_{640GHz})/BT_{640GHz}, in cloud-induced brightness temperature change between the 850- and 664-GHz channel are shown as functions of (a) IWP and column-mean D_{me} and (b) cloud optical depth (τ) and D_{me}, respectively.

channels, while Figure 1d shows the simulated reflectivity profiles "measured" by the 94-GHz radar for the atmosphere along the cross section. We assume nadir viewing for all of the microwave radiometer channels, with a field of view of 15 km × 15 km. The radar reflectivity is simulated at the same horizontal resolution. The decrease of TOA brightness temperature spectra due to cloud particle scattering is clear from Figure 1c. The enhanced radar reflectivity in the convective core where larger ice particles exist is an apparent feature in Figure 1d. These simulated observations directly highlight the sensitivity of the instruments to various types of ice clouds.

3. Sensitivity Studies

For microwave radiometers, sensitivity to ice clouds can be illustrated by the difference between the clear and cloudy TOA brightness temperature, that is, cloud induced change in brightness temperature (BT). Jiang et al. (2017) show the dependence of BT on cloud IWP and column-mean effective diameter (D_{me}) for the frequencies in Table 1 except for the 850-GHz band (Channel 15, Table 1). In this study the sensitivity of the additional channel at 850-GHz channel is examined. A total of 10^6 cases are generated stochastically using the a priori database presented in Jiang et al. (2017) representing various tropical ice cloud types ranging from thin cirrus to deep convection, together with their atmospheric environments. These cases are input into the forward radiative transfer model described in section 2 to calculate the TOA radiance brightness temperature and radar reflectivity vertical profiles. For each case, two calculations are carried out: cloudy radiation and clear-sky radiation by setting cloud water content to zero.

The relative differences in cloud induced change in radiances (BT) between 850 and 664 GHz are illustrated in the two-dimensional space of IWP and D_{me} (Figure 2a), as well as cloud optical depth and D_{me} (Figure 2b). The increase of the BT magnitude in the 850-GHz channel comparing to the 664-GHz channel, the highest frequency of the original TWICE instrument (Jiang et al., 2017), is due to both the IWP (τ) and D_{me}. Larger cloud-induced BT generally indicates an increase in sensitivity to clouds. As shown in Figure 2, the largest impact is apparent for thinner cloud; that is, the addition of the 850-GHz frequency increases the sensitivity of the microwave radiometers to ice clouds that are optically thin ($0.1 < \mathrm{IWP} < 10$ g/m^2, $0.1 < \tau < 1$) and with smaller particles ($20 < D_{me} < 100$ μm). At the same D_{me}, the enhancement in sensitivity to smaller IWP and τ values is also apparent.

To quantitatively assess the vertical resolution and sensitivity of the microwave radiometer suite, an averaging kernel matrix $\boldsymbol{A}$ is calculated for each profile along the cross section using definition below (Rodgers, 2000):

$$A = GK = \mathcal{X}'/\mathcal{X}, \tag{1}$$

where $\mathcal{X}'$ denotes the retrieved variables and $\mathcal{X}$ is the truth state. The Jacobian matrix $\boldsymbol{K}$ is the sensitivity of

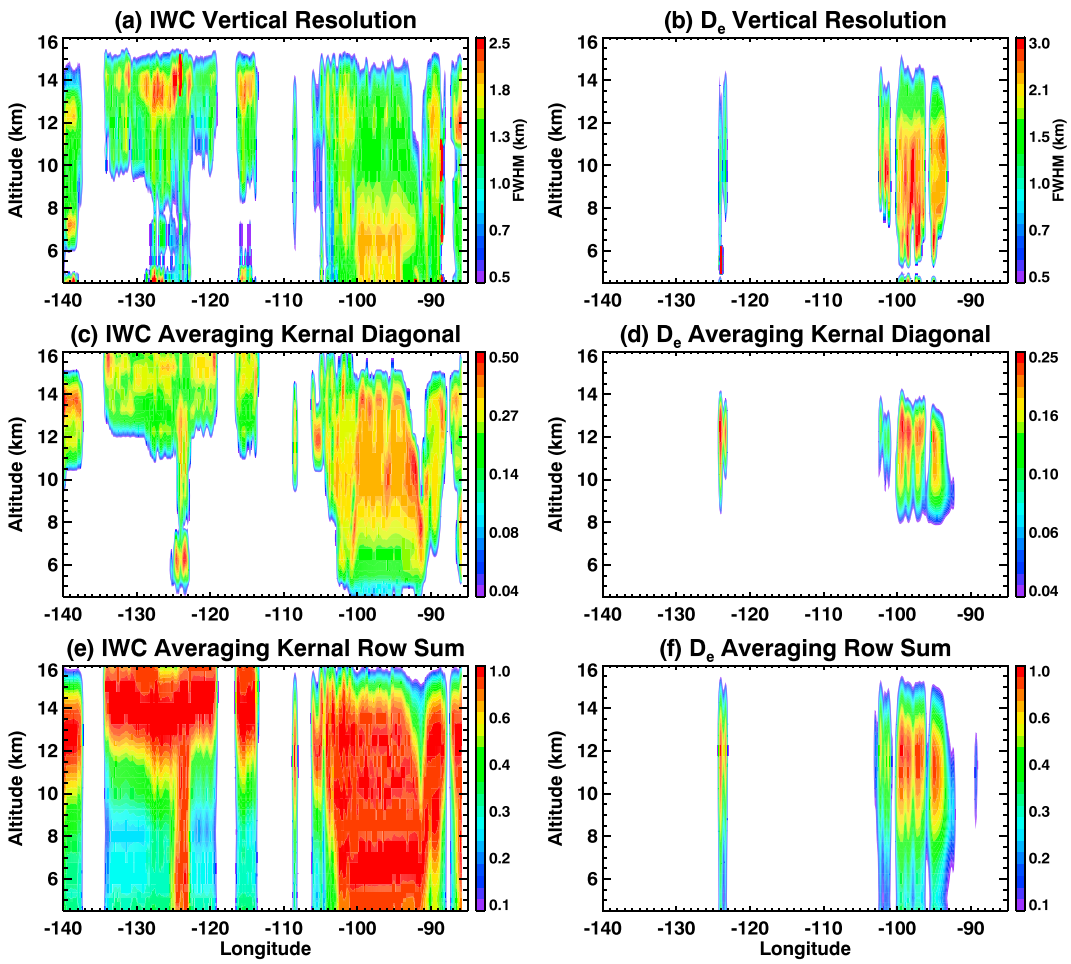

Figure 3. (a and b) The full width at half maximum (FWHM) of the averaging kernel of ice water content (IWC) and D_e, respectively; (c and d) their averaging kernel diagonals; and (e and f) their averaging kernel row sums. The averaging kernel diagonal is a measure of the number of degrees of freedom per vertical level. The averaging kernel row sum is a fraction of how much the retrieval on a vertical level comes from the "observed" radiance data instead of the a priori. All calculations are based on the simulated radiances "observed" by the 15-channel microwave radiometers suite along the cross section at 10°S latitude between 140 and 85°W longitude.

the forward model to $\mathcal{X}$ and is calculated by perturbing each element of $\mathcal{X}$, and $\boldsymbol{G}$ is the gain matrix, which can be calculated by

$$G = \left(K^T s_\epsilon^{-1} K + s_a^{-1}\right)^{-1} K^T s_\epsilon^{-1}, \tag{2}$$

where $\boldsymbol{s}_\epsilon$ is the error covariance matrix of the measured spectrum and $\boldsymbol{s}_a$ is the a priori covariance matrix calculated from cloud measurements made during TC4 (Tropical Composition, Cloud and Climate Coupling) campaign. $\boldsymbol{K}^T$ denotes the transpose of $\boldsymbol{K}$. In the current calculation, $\boldsymbol{s}_\epsilon$ is taken to be proportional to a unit matrix, of the form $\boldsymbol{s}_\epsilon = \sigma_\epsilon^2 \boldsymbol{I}$ with $\sigma_\epsilon = 0.5K$.

The sensitivity of microwave radiometers to cloud profiles can be assessed by the characteristics of IWC and D_e averaging kernel functions ($\boldsymbol{A}$) computed along the cross section (Figure 1) for the 15-channel microwave radiometer suite. The results are illustrated in Figure 3, in which the averaging kernel width (Figures 3a and 3b), diagonal (Figures 3c and 3d), and row sum (Figures 3e and 3f) are shown. The width of $\boldsymbol{A}$ is a measure of the vertical resolution of retrievals and is calculated as the full width at half maximum (FWHM) of $\boldsymbol{A}$. The diagonal of $\boldsymbol{A}$ is a measure of the number of degrees of freedom per vertical level (Rodgers, 2000). The row sum of $\boldsymbol{A}$ is to illustrate how much the retrieval on a vertical level comes from the "observed" radiance data (i.e., instead of the a priori).

The FWHM averaging kernels vary greatly with the background atmosphere. Note that only when the row sum of averaging kernels is larger than 0.2, the FWHM is shown in Figure 3. In general, the 15-channel microwave radiometers suite has high sensitivity to a wide range of IWC profiles spanning from thin cirrus to deep convective ice, although the sensitivity to D_e vertical profiles is reduced below 7 km in deep convection. In general, the FWHM value increases from 0.5 km for IWC and 1 km for D_e near the cloud top to 2-3 km for both IWC and D_e when going deeper inside the clouds, reflecting a broadening of averaging kernels and decreasing of vertical resolution of the IWC and D_e information (and therefore the retrieval as well).

The particle size profile sensitivity is mostly in the anvil and deep convection above 6 km, but with reduced sensitivity to smaller particles in the thin cirrus and near the cloud top. The D_e FWHM are also wider than the IWC FWHM, which increase from about 1 km near the cloud top to 2.5 km at 8- to 11-km altitude.

The results shown in Figure 3 are produced with the 850-GHz channel included. In the Appendix A1, we show the change of averaging kernel FWHM, diagonal and row sum after adding the 850-GHz window channel 15 to the original 14 TWICE channels. The addition of the 850-GHz channel produces narrower averaging kernel functions with larger diagonal elements above 12 km, indicating the increase of profile sensitivity near the cloud top (by 20%). The diagonal and the row sum of D_{me} averaging kernels increase by about 50% and 20%, respectively, indicating the increased information content on D_{me} vertical profile retrieval provided by the new high-frequency channel. In Figure A2, we also illustrate a single-case averaging kernel study, which further confirm that the addition of the 850-GHz channel increases the information content and improves the vertical resolution for both D_{me} and IWC, especially above 12 km.

The vertical resolution of a radar is determined by its pulse length. The 94-GHz cloud radar is assumed to be similar to the CloudSat radar, which has pulse length of 485 m, and ~600 pulses are transmitted per profile. The pulses are oversampled every 240 m. So the result is a radar reflectivity profile with 240-m vertical resolution. However, adjacent bins are not independent. Each bin is correlated with the adjacent bins, and as a result, the actual vertical resolution is ~500 m. The radar reflectivity profiles (Figure 1d) show high sensitivities throughout the vertical profiles of cloud when IWC is greater than ~10 g/m^3 and D_e is greater than ~150 μm; however, very limited or no sensitivity is seen near the cloud top and thin cirrus clouds, where radiometers have better sensitivity.

Figure 4 overlays the truth IWC and D_e profiles that radiometers and the 94-GHz radar will be sensitive to. For radiometers, only cloud layers where the row sum of the radiometer averaging kernels is greater than 0.5 are shown. For the cloud radar, only cloud layers with radar reflectivity larger than -20 dB are shown. These results clearly demonstrate that the combined radar and microwave radiometer instrument suite provide more information than either of them alone, especially for profiling throughout the deep convections.

Our study also found limitations of the combined multifrequency microwave radiometer and cloud radar approach, especially for very small IWC ($\lesssim$0.02 mg/m^3) and D_e ($\lesssim$20 μm), which occurs near convective tops or thin cirrus. Moreover, as shown in Figure 3f, radiometers show very limited information for D_e below 8 km in the deep convection clouds (averaging row sum < 0.5). Therefore, only a single piece of information for particle size in this region is coming from the cloud radar. However, the high information content on IWC from the radiometers (see Figure 3e) can potentially aid the ice particle size retrieval in this region of the clouds. Nevertheless, coordinating observations from instruments like ENTICE and radar with the infrared and visible observations could allow us to further improve ice cloud retrievals [DS2017].

4. Retrieval Simulation

The Bayesian Retrieval Algorithm developed for the TWICE CubeSat (Evans et al., 2012; Jiang et al., 2017) is modified by adding an 850-GHz radiometer channel and a 94-GHz cloud radar. The WRF simulated field in Figure 1 is used as the "truth" data. Vertical profiles of ice cloud as well as atmospheric temperature and water vapor are retrieved from the forward model calculated TOA radiances and radar reflectivity profiles of the "truth" data using the retrieval algorithm discussed in detail by Jiang et al. (2017) and Evans et al. (2012). A hybrid Monte Carlo Integration (MCI) and Levenberg-Marquardt Optimization approach is taken to perform the Bayesian retrieval depending on whether there are enough MCI database points below a threshold value of χ^2, which is given by

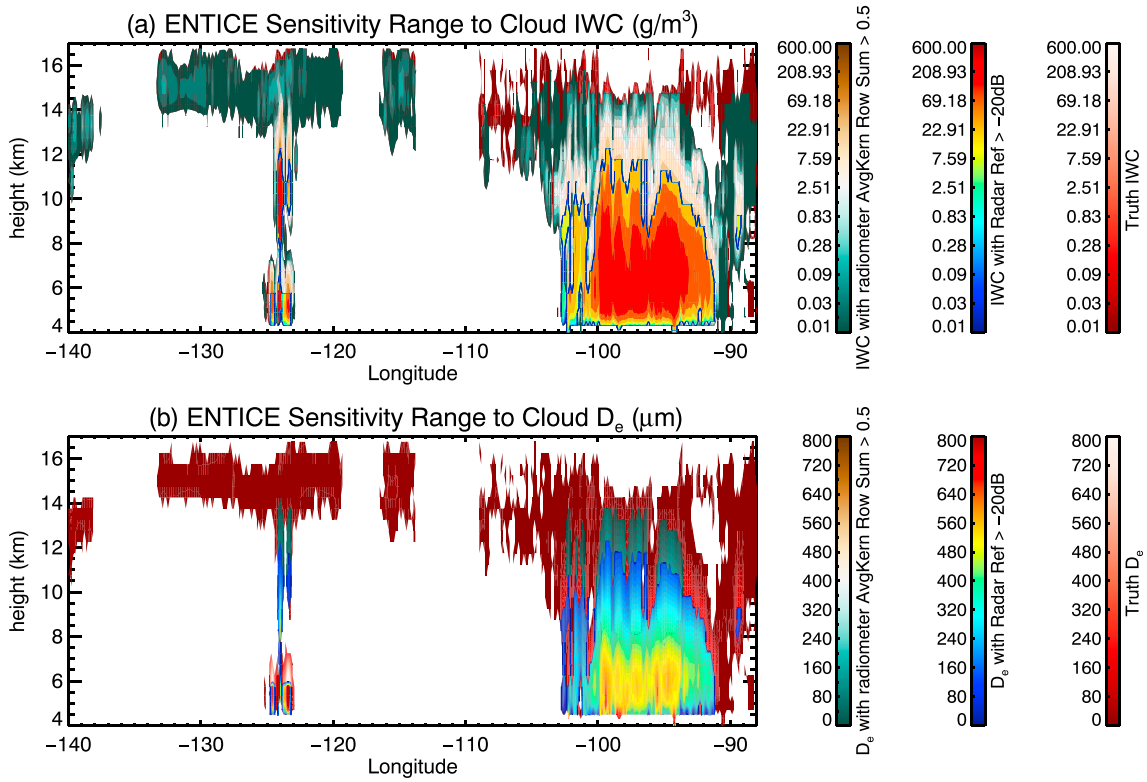

Figure 4. Simulated (a) ice water content (IWC) and (b) D_e profiles overlaid with the sectors in which radiometers and cloud radar have information on shown by different color tables. The distributions of truth IWC and D_e are shown in dark red-white color scale. For radiometer sensitivity, only cloud layers where the row sum of the radiometer averaging kernels is greater than 0.5 are shown (green-brown color scale). For radar sensitivity, only cloud layers with radar reflectivity larger than −20 dB are shown (rainbow color scale).

$$\chi^2 = \sum_{j=1}^{N} \frac{\left(T_j^{\text{sim}} - T_j^{\text{obs}}\right)^2}{\sigma_j}, \tag{3}$$

where T_j^{sim} and T_j^{obs} are the simulated and measured observations, respectively. The Subscript j corresponds to channels at different microwave frequencies with T being the TOA brightness temperature, and to different vertical levels with T being radar reflectivity. A combined measurement and forward modeling uncertainty is given by σ_j, and N is the length of the observation vector. For the microwave radiometer channels, σ_j is assumed to be 1 K, and for the radar, σ_j =1.5 dB including the errors from both the measurement and the radiative transfer modeling. These errors have been added into the simulated observations as independent Gaussian noise of specified root-mean-square (RMS) values (RMS = 1K for radiometers and RMS = 1.5 dB for radar) for each channel.

To simulate the retrieval from a simulated ENTICE observation illustrated in Figure 1, we use both the radiances from the 15 microwave radiometer channels (Table 1 and Figure 1c) and the radar reflectivity (Figure 1d) as the input into the retrieval algorithm. Figures 5 illustrates the performance and accuracy of the retrieval, where the retrieved IWC, D_e, cloud layer (500 m) optical depth τ, RH, and T profiles are shown in the left column, and the retrieval errors computed by comparing with the "truth" profile-by-profile are shown in the middle column. The mean biases (solid line) from all the profiles and the RMS (dashed line) errors are shown in the right column.

The retrieved cloud profiles are limited to altitudes above the freezing level at ~4 km. For clouds with IWC in the range of 0.02 and 3 g/m^3, and D_e larger than 50 μm, the magnitude of mean biases is <40%. For T, the mean retrieval error is within 1 K in the lower troposphere below ~5 km but has up to 2 K cold bias in the midtroposphere and a warm bias above 15 km, which may be related to the fact that the instrument will miss thin (<0.3 optical depth) cloud layers. The mean RH biases are generally within ~20% with an RMS <

10.1029/2019EA000580

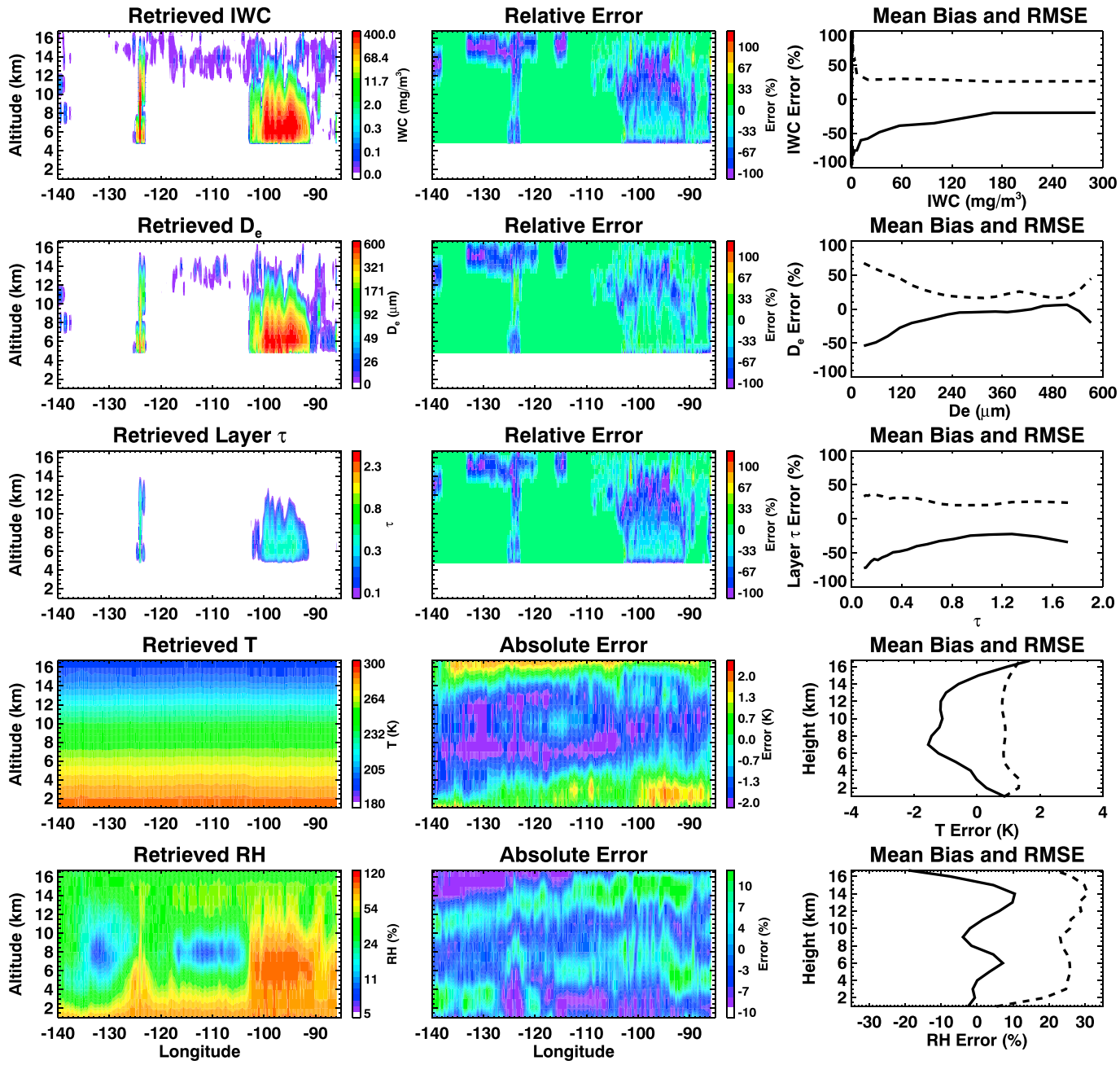

Figure 5. Left column: Retrieved vertical profiles of ice water content (IWC), D_e, cloud layer (500m) optical depth τ, relative humidity (RH), and temperature profiles using the simulated top-of-atmosphere radiances and radar reflectivity profiles along the cross section at 10°S between 140 and 85°W longitude. Middle column: The relative differences, in percent, computed as the retrieved values minus the truth values and then divided by the truth values. Differences for relative humidity and temperature are shown in % and K, respectively. Right column: The mean biases (solid line) and root-mean-square (RMS; dashed line) errors (RMSE) of the mean profiles for the five variables. For IWC, D_e, and τ, histograms of mean errors are presented.

30%. The vertical resolution for the retrieved D_e and IWC is 0.5 km, mainly due to the addition of the 94-GHz radar. The vertical resolution for the retrieved T and RH profiles depends on both the weighting functions and a priori, which are typically coarse at ~3-4 km (Jiang et al., 2017). In general, retrievals underestimate the IWC and D_e especially for IWC < 0.02g/m^3 and D_e < 40 μm, which occurs usually near the cloud top and with thin cirrus clouds. As a result, negative biases as large as -50% are seen for cloud layers with optical depth < 0.3, which is consistent with the sensitivity analysis presented in section 3.

5. Summary and Conclusions

A combined platform of radar and multifrequency passive microwave submillimeter radiometers are recommended by the 2017 Decadal Survey as a candidate measurement approach for the Clouds, Convection and Precipitation (CCP) designated mission.

This study presented a detailed simulation of measurements and their estimated uncertainties from ENTICE's combined radar and multifrequency radiometer package. ENTICE radiometer's frequency channels between 118 and 850 GHz are selected to provide measurement capability for simultaneous retrieved profiles of ice particle effective radius together with IWC, atmospheric moisture. and temperature profiles; ENTICE's 94-GHz cloud radar further enables the retrieval for fine-resolved vertical structure of ice cloud particle effective radius and water content. Compared to the previous TWICE instrument (Jiang et al., 2017), ENTICE increases the vertical resolution of ice cloud retrievals from 3-4 km to 0.5 km and reduces the bias to <40%.

The combined ENTICE radar and radiometer suite significantly improves state-of-the-art measurements [e.g., A-Train; L'Ecuyer & Jiang, 2010] of ice clouds in terms of accuracy, vertical resolution, simultaneous retrieval of atmospheric state (water vapor and temperature), and new ability to retrieve ice cloud particle size. For the first time, it demonstrates a pathway toward the quantification of ice cloud radiative effects and constraining model simulations of ice cloud feedback and associated hydrological processes, contributing to reducing uncertainties of climate predictions. The improved ice cloud measurements by ENTICE will advance our understanding of ice cloud microphysical processes and lead to improved simulations and predictions of severe storms and climate change. Therefore, ENTICE would be an attractive option for future missions targeting clouds, convection, and precipitation processes, as called out in the 2017 Earth Science Decadal Survey by the U.S. National Academies.

Acknowledgments
This work was conducted at the NASA-sponsored Jet Propulsion Laboratory (JPL), California Institute of Technology. We appreciate the support by the JPL's Advanced Concept Funding. This work was partly supported by the NASA Science Mission Directorate, Earth Science Technology Office, as part of the Instrument Incubator Program under grant NNX14AK70G. We thank Frank Evans for his helpful consulting support in radiative transfer modeling and ice cloud retrieval that are applied in this study. The TC4 data that used in our a priori database can be downloaded from the NASA website at https://espo.nasa.gov/tc4/content/TC4. The model simulation data generated from this study are available upon request from the authors. Please contact the corresponding author jonathan.h.jiang@jpl.nasa.gov.

References

Bony, S., Colman, R., Kattsov, V. M., Allan, R. P., Bretherton, C. S., Dufresne, J. L., et al. (2006). How well do we understand and evaluate climate change Feedback Processes? *Journal of Climate*, *19*(15), 3445–3482. https://doi.org/10.1175/JCLI3819.1

Burns, B. A., Wu, X., & Diak, G. R. (1997). Effects of precipitation and cloud ice on brightness temperatures in AMSU moisture channels. *IEEE Transactions on Geoscience and Remote Sensing*, *35*, 1429–1437.

Evans, K. F. (2007). SHDOMPPDA: A radiative transfer model for cloudy sky data assimilation. *Journal of the Atmospheric Sciences*, *64*(2007), 3854–3864. https://doi.org/10.1175/2006JAS2047.1

Evans, K. F., & Stephens, G. L. (1995). Microwave radiative transfer through clouds composed of realistically shaped ice crystals. Part I. Single scattering properties. *Journal of the Atmospheric Sciences*, *52*, 2041–2057.

Evans, K. F., Walter, S. J., Heymsfield, A. J., & Deeter, M. N. (1998). Modeling of submillimeter passive remote sensing of cirrus clouds. *Journal of Applied Meteorology and Climatology*, *37*, 184–205.

Evans, K. F., Wang, J. R., O'C Starr, D., Heymsfield, G., Li, L., Tian, L., et al. (2012). Ice hydrometeor profile retrieval algorithm for high-frequency microwave radiometers: application to the CoSSIR instrument during TC4. *Atmospheric Measurement Techniques*, *5*, 2277–2306. https://doi.org/10.5194/amt-5-2277-2012

Fu, Q., & Liou, K. N. (1992). A three-parameter approximation for radiative transfer in nonhomogeneous atmospheres: Application to the O3 9.6μm band. *Journal of Geophysical Research*, *97*(D12), 13,051–13,058. https://doi.org/10.1029/92JD00999

Hartmann, D. L., & Short, D. A. (1980). On the use of Earth radiation budget statistics for studies of clouds and climate. *Journal of the Atmospheric Sciences*, *37*, 1233–1250.

Hong, G., Heygster, G., Miao, J., & Kunzi, K. (2005). Sensitivity of microwave brightness temperatures to hydrometeors in a tropical deep convective cloud system at 89–190 GHz. *Radio Science*, *40*, RS4003. https://doi.org/10.1029/2004RS003129

Hong, S.-Y., Noh, Y., & Dudhia, J. (2006). A new vertical diffusion package with an explicit treatment of entrainment processes. *Monthly Weather Review*, *134*, 2318–2341. https://doi.org/10.1175/MWR3199.1

Iacono, M. J., Delamere, J. S., Mlawer, E. J., Shephard, M. W., Clough, S. A., & Collins, W. D. (2008). Radiative forcing by long-lived greenhouse gases: Calculations with the AER radiative transfer models. *Journal of Geophysical Research*, *113*, D13103. https://doi.org/10.1029/2008JD009944

Jiang, J. H., Yue, Q., Su, H., Reising, S. C., Kangaslahti, P. P., Deal, W. R., et al. (2017). A simulation of ice cloud particle size, humidity and temperature measurements from the TWICE CubeSat. *Earth and Space Science*, *4*, 574–587. https://doi.org/10.1002/2017EA000296

Kangaslahti, P., E. Schlecht, J.H. Jiang, W. R Deal, A. Zamora, K. Leong, et al. (2016), CubeSat scale receivers for measurement of ice in clouds, 14th Specialist Meeting on Microwave Radiometry and Remote Sensing of the Environment, Espoo, 2016, pp. 42-47, doi: https://doi.org/10.1109/MICRORAD.2016.7530501

L'Ecuyer, T. S., & Jiang, J. H. (2010). Touring the atmosphere aboard the A-Train. *Physics Today*, *63*(7), 36–41. https://doi.org/10.1063/1.3463626

Li, L., Heymsfield, G. M., Racette, P. E., Tian, L., & Zenker, E. (2004). A 94-GHz cloud radar system on a NASA high-altitude ER-2 aircraft. *Journal of Atmospheric and Oceanic Technology*, *21*, 1378–1388. https://doi.org/10.1175/1520-0426

Ogut, M., S. C. Reising, X. Bosch-Lluis, Y. V. Goncharenko, B. Kilmer, P. Kangaslahti, et al., (2018), Design, testing and reliability analysis of command and data handling (C&DH) subsystem for the Tropospheric Water and Cloud Ice (TWICE) instrument for a 6U-Class Small Satellite, *2018 IEEE Geoscience and Remote Sensing Symp*., Fort Worth, TX, pp. 1990-1993, doi: https://doi.org/10.1109/IGARSS.2018.8517952

Reising, S. C, P. Kangaslahti, E. Schlecht, J.H. Jiang, X. Bosch-Lluis, M. Ogut, et al. (2016), Tropospheric water and cloud ICE (TWICE) millimeter and submillimeter-wave radiometer instrument for 6U-Class nanosatellites, 41st International Conference on Infrared, Millimeter, and Terahertz waves, Copenhagen, 2016, pp. 1-2. https://doi.org/10.1109/IRMMW-THz.2016.7758396

Rodgers, C. D. (2000), Inverse methods for remote sounding: Theory and practice, World Sci., Singapore.

Skamarock, W. C., J. B. Klemp, J. Dudhia, D. O. Gill, D. M. Barker, W. Wang, and J. G. Powers (2008), A description of the Advanced Research WRF Version 3., *NCAR Technical* 16 Note TN-468+STR. 113 pp.

Stephens, G. L. (2005). Cloud feedbacks in the climate system: A critical review. *Journal of Climate*, *18*(2), 237–273. https://doi.org/10.1175/JCLI-3243.1

Stephens, G. L., Vane, D. G., Boain, R. J., Mace, G. G., Sassen, K., Wang, Z., et al., & the CloudSat Science Team (2002). The CloudSat mission and the A-Train. *Bulletin of the American Meteorological Society*, *83*(12), 1771–1790. https://doi.org/10.1175/BAMS-83-12-1771

Thompson, G., Field, P. R., Rasmussen, R. M., & Hall, W. D. (2008). Explicit forecasts of winter precipitation using an improved bulk microphysics scheme. Part II: Implementation of a new snow parameterization. *Monthly Weather Review*, *136*, 5095–5115.

Wilheit, T. T., Chang, A. T. C., King, J. L., Rodgers, E. B., Nieman, R. A., Krupp, B. M., et al. (1982). Microwave radiometric observations near 19.35, 92, and 183 GHz of precipitation in tropical storm Cora. *Journal of Applied Meteorology*, *21*(8), 1137–1145. https://doi.org/10.1175/1520-0450(1982)021<1137:MRONAG>2.0.CO;2

Wu, D. and J.H. Jiang (2004), EOS MLS algorithm theoretical basis for cloud measurements, Technical Document, D-19299, Jet Propulsion Laboratory.

Wu, D. L., Jiang, J. H., & Davis, C. P. (2006). EOS MLS cloud ice measurements and cloudy-sky radiative transfer model. *IEEE Transactions on Geoscience and Remote Sensing*, *44*(5), 1156–1165.

Wu, D. L., Jiang, J. H., Read, W. G., Austin, R. T., Davis, C. P., Lambert, A., et al. (2008). Validation of the Aura MLS Cloud Ice Water Content (IWC) Measurements, *Journal of Geophysical Research*, *113*, D15S10. https://doi.org/10.1029/2007JD008931.

Yurkin, M. A., & Hoekstra, A. G. (2011). The discrete-dipole-approximation code ADDA: capabilities and known limitations *Journal of Quantitative Spectroscopy and Radiative Transfer*, *112*(13), 2234–2247. https://doi.org/10.1016/j.jqsrt.2011.01.031

Zhang, C., Wang, Y., & Hamilton, K. (2011). Improved representation of boundary layer clouds over the Southeast Pacific in ARW-WRF using a Modified Tiedtke Cumulus Parameterization Scheme.*Monthly Weather Review*, *139*, 3489–3513. https://doi.org/10.1175/MWR-D-10-05091.1